Available online at www.sciencedirect.com
SCIENCE DIRECT®
Acta Materialia 52 (2004) 5805–5813
Acta MATERIALIA
www.actamat-journals.com

# Effects of reaction heat and self-stress on the transport of hydrogen through metallic tubes under conditions far from equilibrium

Wu-Shou Zhang [a,*], Min-Qiang Hou [a,b], He-Yi Wang [c], Yi-Bei Fu [c]

[a] *Institute of Chemistry and Center for Molecular Science, Chinese Academy of Sciences, P.O. Box 2709, Beijing 100080, PR China*
[b] *Graduate School of the Chinese Academy of Sciences, Beijing 100039, PR China*
[c] *Institute of Nuclear Physics and Chemistry, China Academy of Engineering Physics, Mianyang 621900, PR China*

Received 21 July 2004; received in revised form 25 August 2004; accepted 26 August 2004
Available online 23 September 2004

**Abstract**

A thermokinetic model of hydrogen diffusion across a metallic tube is established. It includes the enthalpy change of the metal–hydrogen reaction, heat losses, dependences of reaction rate and hydrogen diffusion coefficient on temperature, and self-stress effects, etc. A phenomenon, the super fast diffusion of hydrogen before the up-hill diffusion and Fickian diffusion during hydrogen gas charging process, which has been found experimentally for 35 years, is presented by this model. Effects of pressures and other parameters are discussed.


*Keywords:* Hydrides; Hydrogen absorption; Internal stresses; Kinetics; Palladium

## 1. Introduction

Migration of hydrogen interstitials in metals and alloys has been studied widely in science and technology [1–4]. It is well known that a time-lag is necessary for a diffusion wavefront to be detected at the downstream side of a foil while the hydrogen is charged at the upstream side. In 1980s, Lewis et al. found that self-stresses produced by hydrogen insertion into metals and alloys induce the up-hill diffusion (UHD) at the downstream side before the time-lag of the diffusion process [5–17]. Since then, the self-stress effects of hydrogen in metals and alloys have been studied extensively [5–21]. Recently, this phenomenon has been interpreted by the self-stress theories in thin shells and plates [22–25]. However, another anomalous phenomenon of hydrogen transport has been found for 35 years, which has not attracted much attention and which was misinterpreted in past works. It is that the hydrogen pressure inside a tube increases (or decreases) almost simultaneously with the outer $H_2$ gas pressure increasing (or decreasing) [13–17,26], we call it super fast diffusion (SFD); it lasts a very short time and appears before the UHD and Fickian diffusion waves. However, this phenomenon does not occur in processes of electrochemical charging and discharging [5–12].

Hickman [26], Lewis and coworkers [13,14] have explained the SFD as a result of external stress induced by the outer pressure imposed during hydrogen charging and it was named as "mechanically induced memory effects". Although external stress does exists under gas charging, our analysis indicates this effect is too small to explain the SFD. On the other hand, the self-stress theory for free-plates of metal–hydrogen system has

* Corresponding author. Tel.: +86 106 255 4276; fax: +86 106 255 9373.
*E-mail address:* wszhang@iccas.ac.cn (W.-S. Zhang).

1359-6454/$30.00 
doi:10.1016/j.actamat.2004.08.038

presented this effect [27], however, it cannot explain other phenomena, e.g., UHD in electrochemical charging, the time course of internal pressure change, and the acceleration of permeation rate on interruption of hydrogen charging [5–12].

In this paper, we will interpret the SFD by a thermokinetic model. The reaction energy of hydrogen absorption heats up the metallic tube and causes the tube wall to desorb hydrogen at the downstream side; therefore the pressure inside the tube increases at the beginning of hydrogen charging. A similar process exists during hydrogen discharging.

## 2. Model

Consider a vertical metallic tube with the bottom sealed and the top connected to a glass tube [6,17], which is open to a gauge for pressure measurement as presented in Fig. 1. Similarly to previous works [22,24], we use a one-dimensional model to simulate the actual processes, the coordinate $z$ is along the thickness direction; the outer and inner surfaces of the metallic tube wall (MTW) are at $z = 0$ and $L$, respectively.

The stress in MTW is [22]:

$$\sigma = \frac{2V_{\mathrm{H}}EC_0}{3(1-\nu)}(\bar{n}_{\mathrm{H}} - n_{\mathrm{H}}) - \frac{3r}{2L}(p_{\mathrm{out}} - p_{\mathrm{in}}), \tag{1}$$

with

$$\bar{n}_{\mathrm{H}} = \frac{1}{L}\int_0^L n_{\mathrm{H}}\,\mathrm{d}z, \tag{2}$$

where $n_{\mathrm{H}}$ is the atomic ratio of hydrogen to metal (M); $C_0$ is the concentration of H in M corresponding to $n_{\mathrm{H}} = 1$, $C_0 = 0.113\ \mathrm{mol\,cm^{-3}}$ for Pd; $V_{\mathrm{H}}$ is the partial molar volume of H in M, $V_{\mathrm{H}} = 1.6\ \mathrm{cm^3}$ for fcc metals and alloys [28,29]; $E$ and $\nu$ are Young's modulus and Poisson's ratio of the metal, respectively; $r$ is the radius of tube; $p_{\mathrm{out}}$ and $p_{\mathrm{in}}$ are the pressures outside and inside the tube, respectively. The first term on the right-hand-side of Eq. (1) is the self-stress produced by hydrogen insertion [22]; the second term is caused by the external static load (pressure difference here) on thin cylindrical shells [30].

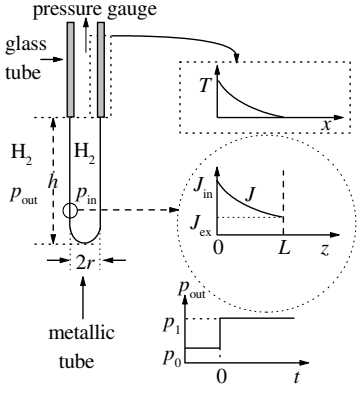


Fig. 1. Schematic picture of hydrogen gas absorption into a metallic tube.

The hydrogen diffusion flux for the dilute solid-solution phase of H in M has the form [22]:

$$J(z,t) = -D_0\exp\left(-\frac{E_{\mathrm{a}}}{RT}\right)C_0\left[1 + n_{\mathrm{H}}(1-n_{\mathrm{H}})\frac{2V_{\mathrm{H}}^2EC_0}{3(1-\nu)RT}\right]\frac{\partial n_{\mathrm{H}}}{\partial z}, \tag{3}$$

where $D_0\exp(-E_{\mathrm{a}}/RT) = D(T)$ is the diffusion coefficient of H in M at temperature $T$ in K, $D_0$ and $E_{\mathrm{a}}$ are the pre-exponential factor and activation energy, respectively, and $R$ is the molar gas constant.

Applying the mass balance condition to the flux expression of Eq. (3) yields:

$$C_0\frac{\partial n_{\mathrm{H}}}{\partial t} = -\frac{\partial J(z,t)}{\partial z}, \tag{4}$$

with boundary conditions:

$$J_{\mathrm{in}} = J(0,t) \quad \text{and} \quad J_{\mathrm{ex}} = J(L,t), \tag{5}$$

where the input and output fluxes are expressed as:

$$J_{\mathrm{in}} = k_{0,+}\exp\left(-\frac{\Delta E_{0,+} - V_{\mathrm{H}}\sigma}{RT}\right)p_{\mathrm{out}}(1-n_{\mathrm{H}})^2 - k_{0,-}\exp\left(-\frac{\Delta E_{0,-} + V_{\mathrm{H}}\sigma}{RT}\right)n_{\mathrm{H}}^2, \quad z = 0 \tag{6}$$

and

$$J_{\mathrm{ex}} = k_{L,-}\exp\left(-\frac{\Delta E_{L,-} + V_{\mathrm{H}}\sigma}{RT}\right)n_{\mathrm{H}}^2 - k_{L,+}\exp\left(-\frac{\Delta E_{L,+} - V_{\mathrm{H}}\sigma}{RT}\right)p_{\mathrm{in}}(1-n_{\mathrm{H}})^2, \quad z = L, \tag{7}$$

respectively. In Eqs. (6) and (7), $k$ is the rate constant of the M–$H_2$ reaction: $\frac{1}{2}n_{\mathrm{H}}\mathrm{H}_2 + \mathrm{M} \leftrightarrow \mathrm{MH}_{n_{\mathrm{H}}}$, $\Delta E$ is the activation energy; $n_{\mathrm{H}}$ and $\sigma$ take values just below the surface ($z = 0$ or $L$); subscripts 0 and $L$ are for $z = 0$ and $L$, respectively; subscripts + and − are for reactions of hydrogen absorption and desorption, respectively. At equilibrium, these two equations are equivalent to:

$$\frac{n_{\mathrm{H}}}{1-n_{\mathrm{H}}} = b\exp\left(-\frac{\Delta H - V_{\mathrm{H}}\sigma}{RT}\right)p^{1/2}, \tag{8}$$

with

$$b = \sqrt{\frac{k_{0,+}}{k_{0,-}}} = \sqrt{\frac{k_{L,+}}{k_{L,-}}} \tag{9}$$

and

$$\Delta H = \frac{\Delta E_{0,+} - \Delta E_{0,-}}{2} = \frac{\Delta E_{L,+} - \Delta E_{L,-}}{2}, \tag{10}$$

where $\Delta H$ is the enthalpy change of the hydrogen absorption reaction. Eqs. (6) and (7) are the simplest expressions for the M–$H_2$ reaction, steps of $H_2$ molecules adsorption and dissociation on the metal surface and penetration of H atoms from the surface into the bulk are incorporated into a single step. Eq. (8) is the isotherm of hydrogen absorption by fcc metals or alloys under stress $\sigma$ [4,7,29], $b\exp(-\Delta H/RT)$ is the Sieverts parameter.

The pressure change inside the tube is:

$$\Delta p = p_{\text{in}} - p_0 = \frac{T - T_0}{T_0} p_0 + \frac{RTA_{\text{M}}}{2V_{\text{g}}} \int J_{\text{ex}}\,\mathrm{d}t, \tag{11}$$

where $T$ is the temperature of MTW and gas inside the tube; $p_0$ and $T_0$ are initial values of $p$ and $T$, respectively; $A_{\text{M}} = 2\pi rh$ is the area of MTW; $h$ is the tube height; $V_{\text{g}}$ is the collection volume in which hydrogen gas is sealed.

The energy balance equation of the MTW is:

$$V_{\text{M}} c_{\text{M}} \frac{\mathrm{d}T}{\mathrm{d}t} = -A_{\text{M}} \int_0^L \Delta H \frac{\partial n_{\text{H}}}{\partial z}\,\mathrm{d}z - A_{\text{M}}\alpha(T - T_0) - A_{\text{M}}\varepsilon_{\text{M}}\sigma_{\text{S-B}}(T^4 - T_0^4) - 2\pi r_{\text{G}} L_{\text{G}} j_{\text{G}}, \tag{12}$$

where $V_{\text{M}} = 2\pi rLh$ is the volume of MTW; $c_{\text{M}}$ is the specific heat of MTW, $c_{\text{M}} = 2.47$ to $2.94\ \text{J cm}^{-3}\ \text{K}^{-1}$ for Pd, Ag and Pt, therefore, $c_{\text{M}}$ of their alloys used experimentally [13–17] has a value around this range; $\alpha$ is the transfer factor of thermal convection; $\varepsilon_{\text{M}}$ is the total emittance of metallic tube surface, we choose the value of Pt black, $\varepsilon_{\text{M}} = 0.91$ [31], as that of Pd black coated on the surface [13–17]; $\sigma_{\text{S-B}} = 5.67032 \times 10^{-12}\ \text{W cm}^{-2}\ \text{K}^{-4}$, the Stefan–Boltzmann constant; $r_{\text{G}}$, $L_{\text{G}}$, $2\pi r_{\text{G}} L_{\text{G}}$ are radius, thickness and cross-section of glass tube wall (GTW); $j_{\text{G}}$ is the thermal flux in the GTW near the top of MTW ($x = 0$ in Fig. 1).

On the right-hand side of Eq. (12), the first term is the heat power produced by exothermic reaction of hydrogen absorption; the second one is the heat loss on surface by natural convection; the third term is the radiation power; the fourth term is the heat loss along the axial direction by thermal conduction in the GTW. The isothermal assumption within tube is used in Eq. (12) since the relaxation time of thermal transport in MTW is much less than that in GTW or that of hydrogen diffusion in MTW. At the same time, thermostresses in MTW are omitted because of the same reason.

The heat transfer factor in Eq. (12) has the form:

$$\alpha = Nu \frac{\lambda_{\text{g}}}{h}, \tag{13}$$

with

$$Nu = cRa^n \tag{14}$$

and

$$Ra = \frac{2\rho_{\text{g}}^2 c_{\text{g}} g (T - T_0) h^3}{\eta_{\text{g}} \lambda_{\text{g}} (T + T_0)}, \tag{15}$$

where $Nu$ and $Ra$ are Nusselt and Rayleigh numbers, respectively; constants $c$ and $n$ depend on the magnitude of $Ra$ [32], $c = 1.18$, $n = 1/8$ for $10^{-2} \leqslant Ra < 10^4$ and $c = 0.54$, $n = 1/4$ for $10^4 \leqslant Ra < 10^9$, there is no value of $Ra$ greater than $10^9$ in this model; $g$ is the gravitational acceleration; $\eta_{\text{g}}$ is the absolute viscosity of $H_2$ gas; $\lambda_{\text{g}}$ is the thermal conductivity of $H_2$ gas; $\rho_{\text{g}}$ is the density of $H_2$ gas; $c_{\text{g}}$ is the specific heat of $H_2$ gas.

For convenience, quantities changing with temperature and pressure in Eq. (15) are expressed as reduced values relative to those at normal temperature and pressure (25 °C, 1 atm), thus we have [33]:

$$\rho_{\text{g}} = \rho_{\text{g,N}} \frac{T_{\text{N}}}{T_0} \frac{p_{\text{out}}}{p_{\text{N}}}, \tag{16}$$

$$\eta_{\text{g}} = \eta_{\text{g,N}} \sqrt{\frac{T_0}{T_{\text{N}}}}, \tag{17}$$

$$\lambda_{\text{g}} = \lambda_{\text{g,N}} \sqrt{\frac{T_0}{T_{\text{N}}}}, \tag{18}$$

where the quantities with the subscript N indicate the values at normal temperature and pressure. The heat convection in Eq. (12) can be expressed as

$$\alpha(T - T_0) = \text{C}_{\text{g}} \left(\frac{h}{h_{\text{N}}}\right)^{3n-1} \left(\frac{T_{\text{N}}}{T_0}\right)^{3n-1/2} \left(\frac{p_{\text{out}}}{p_{\text{N}}}\right)^{2n} \frac{(T - T_0)^{n+1}}{(T + T_0)^n}, \tag{19}$$

with

$$C_{\text{g}} = c \left[\frac{2\rho_{\text{g,N}}^2 c_{\text{g}} g h_{\text{N}}^3}{\eta_{\text{g,N}} \lambda_{\text{g,N}}}\right]^n \frac{\lambda_{\text{g,N}}}{h_{\text{N}}}, \tag{20}$$

where $\rho_{\text{g,N}} = 8.234 \times 10^{-5}\ \text{g cm}^{-3}$, $g = 979.75\ \text{cm s}^{-2}$, $c_{\text{g}} = 14.301\ \text{J g}^{-1}\ \text{K}^{-1}$, $h_{\text{N}} = 1\ \text{cm}$, $\eta_{\text{g,N}} = 8.93 \times 10^6\ \text{Pa s}$, $\lambda_{\text{g,N}} = 1.81 \times 10^{-3}\ \text{W cm}^{-1}\ \text{K}^{-1}$. Therefore, $C_{\text{g}} = 5.12 \times 10^{-3}\ \text{W cm}^{-2}\ \text{K}^{-1}$ for $10^{-2} \leqslant Ra < 10^4$ and $C_{\text{g}} = 5.62 \times 10^{-3}\ \text{W cm}^{-2}\ \text{K}^{-1}$ for $10^4 \leqslant Ra < 10^9$. Combining Eqs. (15)–(18) and above quantities, we have:

$$Ra = 1095.45 \left(\frac{h}{h_{\text{N}}}\right)^3 \left(\frac{T_{\text{N}}}{T_0}\right)^3 \left(\frac{p_{\text{out}}}{p_{\text{N}}}\right)^2 \frac{T - T_0}{T + T_0} \tag{21}$$

for $H_2$ gas.

The energy balance equation in GTW is

$$\frac{\partial T}{\partial t} = -a_{\text{G}} \frac{\partial^2 T}{\partial x^2} - \frac{\alpha}{L_{\text{G}} c_{\text{G}}} (T - T_0) - \frac{\varepsilon_{\text{G}} \sigma_{\text{S-B}}}{L_{\text{G}} c_{\text{G}}} (T^4 - T_0^4), \tag{22}$$

with boundary conditions:

$$\begin{aligned} &j_{\text{G}} = -a_{\text{G}} c_{\text{G}} \tfrac{\partial T}{\partial x}, \quad x = 0, \\ &T = T_0, \quad x = h_{\text{G}}, \end{aligned} \tag{23}$$

where $x$ is the coordinate along the axial direction as shown in Fig. 1; $a_{\text{G}} = 3.4 \times 10^{-3}\ \text{cm}^2\ \text{s}^{-1}$ and $c_{\text{G}} = 2.2$

J cm$^{-3}$ K$^{-1}$ are the thermal diffusion coefficient and specific heat of glass, respectively. $\alpha(T-T_0)$ corresponds to the thermal convection around GTW same as that in Eqs. (12) and (19); the third term corresponds to the radiation; $\varepsilon_G = 0.94$ is the total emittance of glass [31].

The initial condition is the homogenous distribution of hydrogen concentration in MTW, equilibrium of hydrogen chemical potential is reached between the solid and gas phases before the initial time ($t = 0$), when the external hydrogen pressure changes from $p_0$ to $p_1$ as presented in Fig. 1:

$$p_{out} = p_{in} = p_0; \quad T = T_0, \quad n_H = n_{H,0}, \quad \sigma = 0, \quad t < 0, \\ p_{out} = p_1, \quad t \geqslant 0, \tag{24}$$

where $n_{H,0}$ corresponds to $p_0$ and $T_0$ according to Eq. (8).

For comparison, we also discuss the situation of electrochemical charging. The internal stresses and boundary conditions are the same as before, the M–$H_2$ surface process is replaced by the Pd–H electrode reaction as treated earlier [22,24,34]; the only emphasized point here is that the heat convection in Eqs. (12) and (22) being replaced by

$$\alpha(T-T_0) = C_w\left(\frac{h_G}{h_N}\right)^{3n-1}\frac{(T-T_0)^{n+1}}{(T+T_0)^n}, \tag{25}$$

with

$$C_w = c\left[\frac{2\rho_w^2 c_w g h_N^3}{\eta_w \lambda_w}\right]^n \frac{\lambda_w}{h_N}, \tag{26}$$

where $\rho_w = 1$ g cm$^{-3}$, $c_w = 4.181$ J g$^{-1}$ K$^{-1}$, $\eta_w = 8.554\times10^{-4}$ Pa s and $\lambda_w = 6.104\times10^{-3}$ W cm$^{-1}$ K$^{-1}$ at room temperature. Therefore, $C_w = 7.62\times10^{-2}$ W cm$^{-2}$ K$^{-1}$ for $10^{-2} \leqslant Ra < 10^4$ and $C_w = 0.369$ W cm$^{-2}$ K$^{-1}$ for $10^4 \leqslant Ra < 10^9$. The corresponding Rayleigh number is:

$$Ra = 1.5691\times10^8\left(\frac{h_G}{h_N}\right)^3\frac{T-T_0}{T+T_0} \tag{27}$$

for $H_2O$.

In this work, we present results of a numerical procedure reported earlier [34], where the various differential equations are solved by a finite difference method. In the calculation, the time step is $10^{-4}$ and the space step is $10^{-2}$, the precision is $10^4$.

## 3. Results

An example of hydrogen gas charging process is shown in Fig. 2. The initial and applied $H_2$ pressures correspond to $n_H = 0.145$ and 0.545 at room temperature, respectively; dimensions of MTW are taken from [13–17]. From Fig. 2(a), we find that the internal pressure changes simultaneously with outer pressure applied and it increases firstly up to a maximum value then decreases to a minimum less than the initial pressure because of UHD, finally the internal pressure rise monotonically. This physical picture is the same as found experimentally [13–17].

There are three factors, the heat production and loss, the self-stress and the concentration gradient of H in M, competing and inducing the complicated behavior of the pressure change. At the start, the MTW absorbs hydrogen at upstream; this exothermic reaction heats up the MTW as shown in Fig. 2(d). The heated MTW desorbs hydrogen at downstream in a very short initial time as illustrated in the insert in Fig. 2(b). The temperature increase and output flux together modify the internal pressure as indicated in Eq. (11). For the maximum value of pressure change in Fig. 2(a), contributions from temperature increment and hydrogen desorption are 17% and 83%, respectively. After some time, the heat dissipation exceeds the heat production and the tube temperature begins to decrease as presented in Fig. 2(c) and (d).

When the temperature increases slowly, the self-stress effect dominates the kinetics of hydrogen transport. The MTW absorbs hydrogen through its inner surface as discussed previously [22], therefore the direction of $J_{ex}$ changes and the internal pressure decreases as shown in Fig. 2(b) and (a), respectively. After an enough long time, the flux wavefront of hydrogen interstitials reaches the downstream, Fickian behavior dominates the transport kinetics and the pressure increase monotonically (see Fig. 2(a) and (b)).

Fig. 2(c) shows the heat dissipation and shares of different contributions, the heat dissipation is proportional to the temperature difference between the tube and environment as expected. Although contributions from convection, radiation and conduction vary with time in the overall process, they approach stable values of 53%, 41% and 6% of the overall heat dissipation, respectively, after a short initial time. These results also indicate that the length of the glass tube does not affect the qualitative characteristics of pressure change because the thermal diffusion coefficient of glass is a negligible value.

Fig. 3 shows effects of initial and applied pressures on SFD, it is found that the maximum amplitude of $\Delta p/p_0$ in SFD decreases with $p_0$ while $p_1$ is fixed (see Fig. 3(a)) because the corresponding hydrogen content step on the outer surface decreases; however, the absolute change of maximum $\Delta p$ in SFD, $\Delta p_{max}$, has the maximum value at $p_0 = 30.4$ Torr as shown in the insert in Fig. 3(a) and $\Delta p_{max}$ may increase or decrease with $p_0$ in different ranges of initial pressure as observed experimentally [15]. The amplitude of $\Delta p/p_0$ in SFD increases with rising of $p_1$ because the hydrogen content rises on the outer surface as illustrated in Fig. 3(b) and demonstrated experimentally [14].

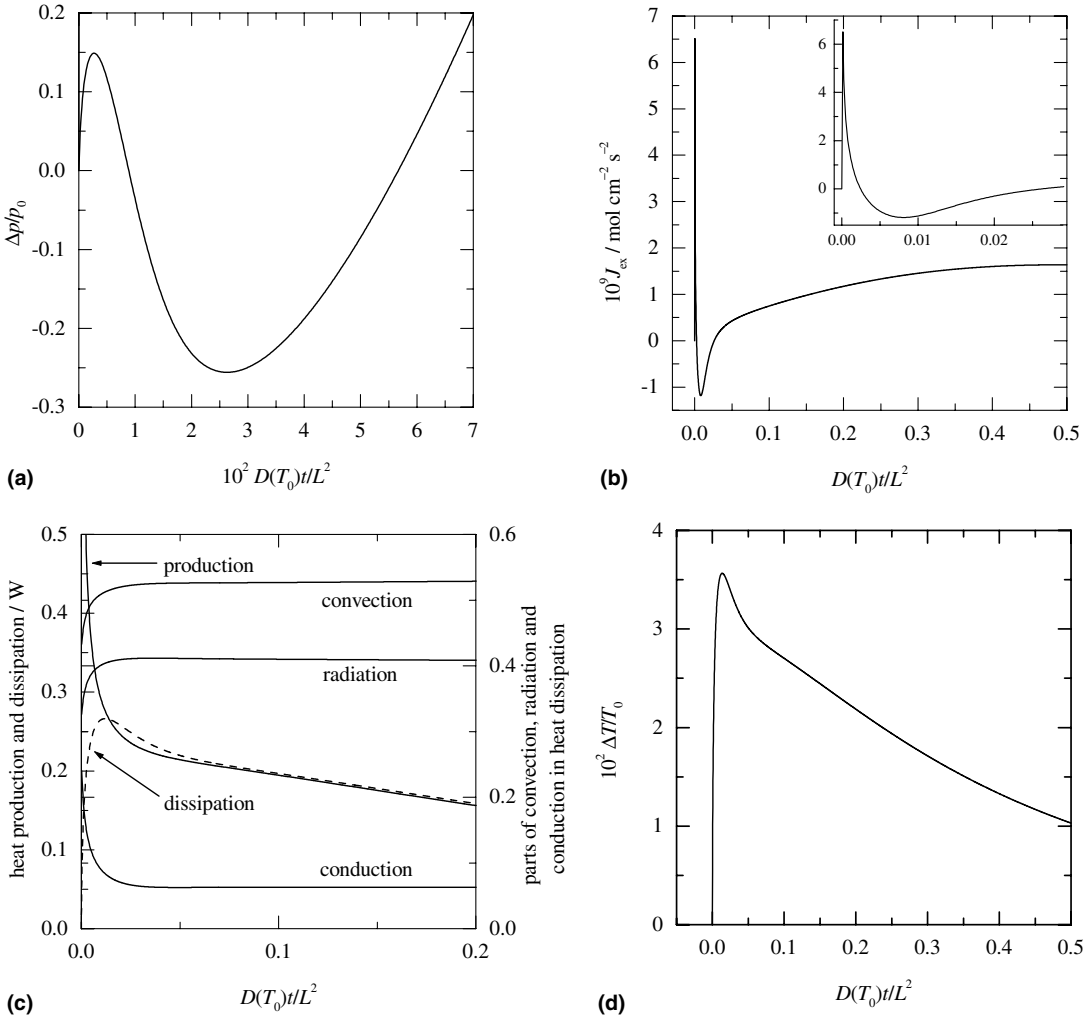


Fig. 2. An example of hydrogen gas absorption into a metallic tube: (a) Pressure change inside tube; (b) the output flux at downstream side; (c) the heat production and dissipation, and parts of different contributions to heat dissipation; (d) temperature change of the metallic tube. The parameters are: $r = 0.4$ cm, $L = 0.04$ cm, $h = 7$ cm; $V_g = 23$ cm$^3$, $p_0 = 2$ Torr, $p_1 = 100$ Torr, $T_0 = 298.15$ K; $D_0 = 1.5 \times 10^{-3}$ cm$^2$ s$^{-1}$, $E_a = 22$ kJ mol$^{-1}$, $2V_H^2 EC_0/3(1-v) = 50$ kJ mol$^{-1}$; $\Delta E_{0,+} = \Delta E_{L,+} = 25$ kJ mol$^{-1}$, $\Delta E_{0,-} = \Delta E_{L,-} = 75$ kJ mol$^{-1}$; $k_{0,+} = 1$ mol cm$^{-2}$ s$^{-1}$ torr$^{-1}$,$k_{L,+} = 1$ mol cm$^{-2}$ s$^{-1}$ Torr$^{-1}$, $b = 5 \times 10^{-6}$ Torr$^{-1/2}$, $k_{0,-}$ and $k_{L,-}$ are deduced from Eq. (9); $c_M = 2.7$ J cm$^{-3}$ K$^{-1}$; $a_G = 3.4 \times 10^{-3}$ cm$^2$ s$^{-1}$, $c_G = 2.2$ Jcm$^{-3}$ K$^{-1}$; $r_G L_G / rL = 2$, $h_G = 15$ cm.

Fig. 4 shows effects of various parameters on the SFD and UHD. Firstly, we discuss influences of the heat transfer factor in natural convection. Because Eq. (19) is only suitable for a vertical tube with infinite length, it is applied here by using $l/r = 17.5$. We change the value of $C_g$ in Eq. (19) two times, i.e., the value of $C_g$ is 1/2 or 2 times of that in Eq. (20). It is found that the qualitative characteristics are the same as Fig. 2(a) because the convection is only a part of heat dissipation as demonstrated in Fig. 2(c). The only difference is the magnitude of SFD and UHD, this means that a strong convection suppresses the SFD and enhances the UHD.

Fig. 4(b) shows influences of the rate constant of the outer surface reaction on the SFD and UHD. Low values of the rate constant, which correspond to deactivated outer surfaces of MTW, reduce the absorption rate, changes of temperature and hydrogen concentration in MTW remarkably. Therefore, effects of SFD and UHD are not prominent. This conclusion is consistent with experimental results, i.e., the SFD and UHD only appear when sample surfaces are catalytically activated by electrodeposition of palladium black [14]; otherwise, it is difficult to observe both effects if the surface is deactivated by immersions of sample in a solution of $I_2$ in KI [14].

Fig. 4(c) shows effects of the hydrogen diffusion coefficient on the SFD and UHD. For large diffusion coefficients, we find that the SFD is prominent and the UHD may be concealed by the SFD as was shown by experimental results [26]. Otherwise, the SFD disappears and UHD is prominent while hydrogen diffusion coefficient

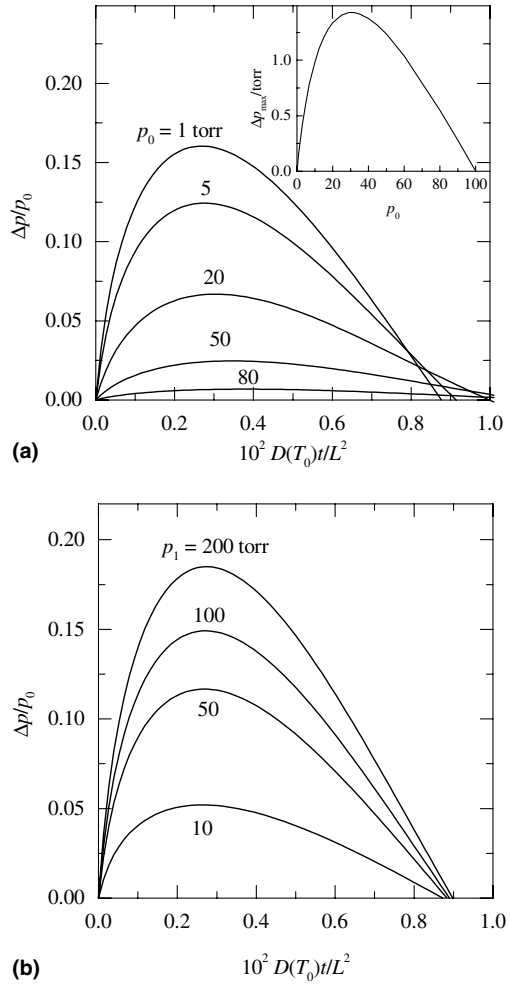


Fig. 3. Effects of initial (a) and applied (b) pressures on SFD. The parameters are the same as those in Fig. 2 except the ones shown as labels in this figure.

decreases due to the reaction heat has enough time to dissipate.

Influences of the MTW thickness are similar to that of the diffusion coefficient as shown in Fig. 4(d). For a thin tube wall, the temperature rises drastically and the UHD is concealed by the SFD; therefore, only tubes with suitable thickness may exhibit both SFD and UHD clearly.

Fig. 5 shows a trivial situation with initially hydrogen-free wall ($n_{H,0} = 0$). We find that both SFD and UHD phenomena all vanish as observed experimentally [17], the only difference is that the diffusion is faster for practical situation than the isothermal assumption.

In experiments, the SFD only appears in gas charging processes and it has not yet been observed during electrochemical charging [5–12]. To compare these two situations, we simulate the electrochemical charging in Fig. 6 with the electrochemical reaction and boundary conditions as discussed earlier [34]. We find that the maximum increment of temperature, $\Delta T/T_0 = 4.73 \times 10^{-3}$ is much less than $3.57 \times 10^{-2}$ in Fig. 2(d) by 7.5 times for the reason that the heat loss is much faster for water than hydrogen gas. Of course, there is a very small increment of pressure, $\Delta p/p_0 = 2.75 \times 10^{-3}$ after short time, $D(T_0)t/L^2 = 9.31 \times 10^{-5}$ as shown in the insert in Fig. 6 and this small SFD is generally neglected experimentally. Therefore, only the UHD effect is prominent in electrochemical charging experiments [5–12] and the SFD effect is notable in gas charging processes [13–17].

Comparing Fig. 2(a) with Fig. 6, we find that the hydrogen transport is generally faster in gas charging than in electrochemical charging because of temperature increasing. Similar difference occurs between the non-isothermal and isothermal situations in Fig. 5. These results mean that measured diffusion coefficients may be greater than the actual one in charging process. It is also indicated that the induced hydrogen concentration step must be small enough in diffusion coefficient measurements so that the heat release and self-stress effect are not prominent; otherwise, the isothermal assumption is not always satisfied.

The SFD has been associated with the net pressure difference across the MTW [13,14,26]. To simulate this effect, we consider an additional 100 Torr pressure of inert gas (e.g., argon gas in [14]) being applied to the outer surface of tube with initial $H_2$ pressure of 2 Torr. It is found that the MTW desorbs hydrogen and the internal pressure increases under the external compressive stress as expected, however, the maximum $\Delta p/p_0$ is much smaller than that in Fig. 2(a) by three orders of magnitude and cannot match experimental results in [13–17]. Besides the external-stress, another factor is the pure mechanical effect, i.e., an external pressure makes the MTW shrink and the internal volume $V_g$ decrease, and then the internal pressure increases. However, the maximum amplitude of pressure change is less than that in Fig. 2(a) by six orders of magnitude and this effect has been verified experimentally using argon gas [14].

We also find that the SFD occurs in the hydrogen desorption process as observed experimentally [13–17]. The physical picture is similar to that in charging processes and it will not be discussed in detail.

## 4. Comparison with experimental results

In order to test the validity of the present treatment, we compare the theoretical results with experimental data. There is much evidence indicating the existence of SFD [13–17,26], we chose one that has enough data for our analysis as is plotted in Fig. 7. In this figure, we use a simpler model than that in the above section, the last term on the right-hand-side of Eq. (12) is removed because GTWs contribution to heat loss is small as shown in Fig. 2(c); and the heat transfer factor in Eq. (12) takes a fixed value but not the form of

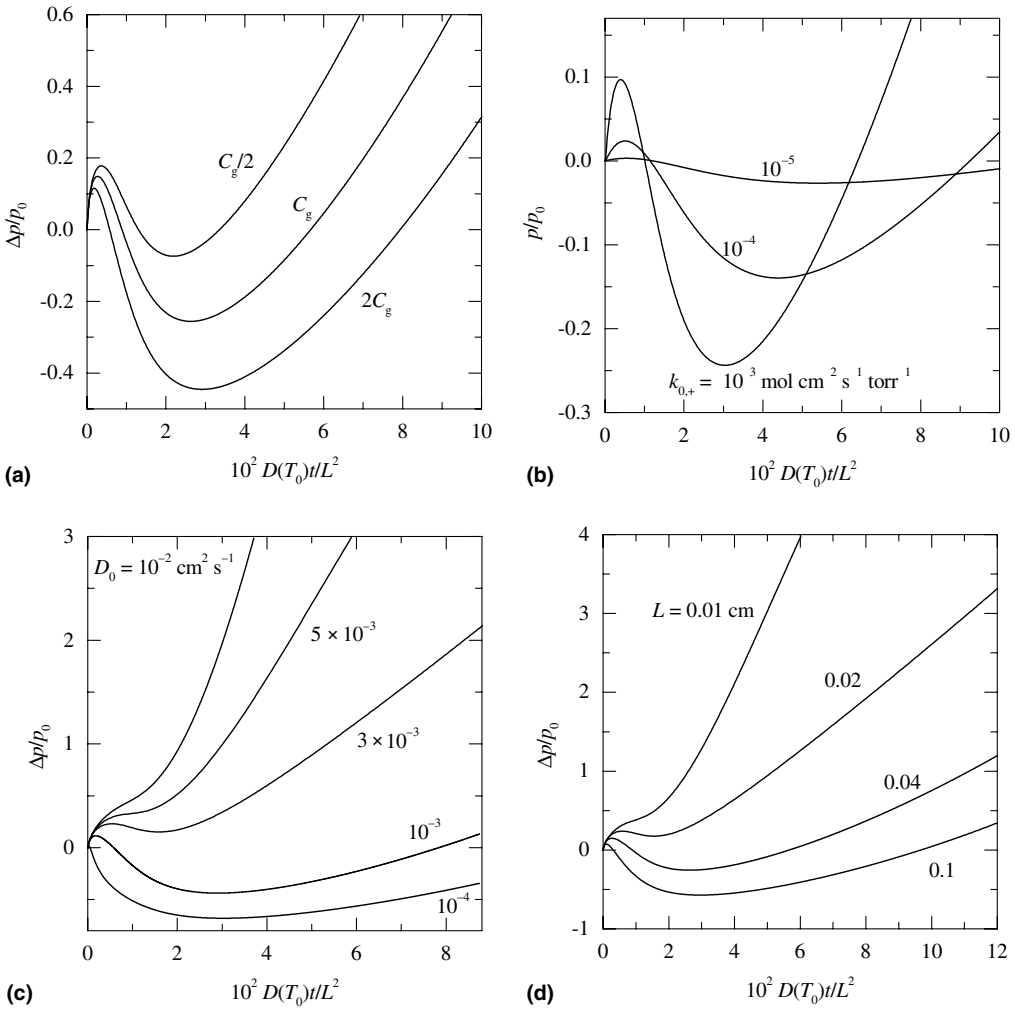


Fig. 4. Effects of heat transfer factor (a), rate constant (b), hydrogen diffusion coefficient (c) and MTW thickness (d) on the SFD and UHD. The parameters are the same as those in Fig. 2 and Eq. (20) except the value shown as labels.

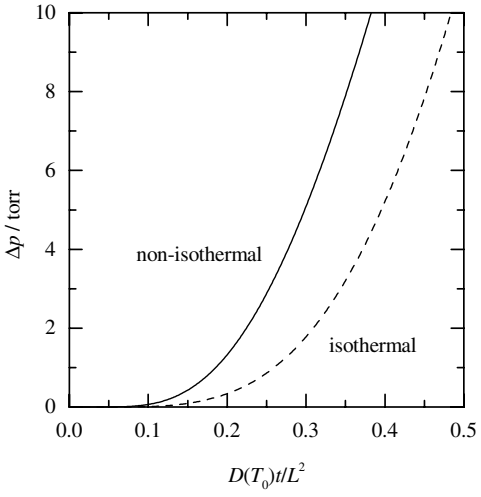


Fig. 5. Effect of heat production on hydrogen diffusion with initial condition of zero hydrogen content in the tube wall, the dash curve is the result under the isothermal assumption. The parameters are the same as those in Fig. 2 except the initial pressure of $p_0 = 0$ Torr.

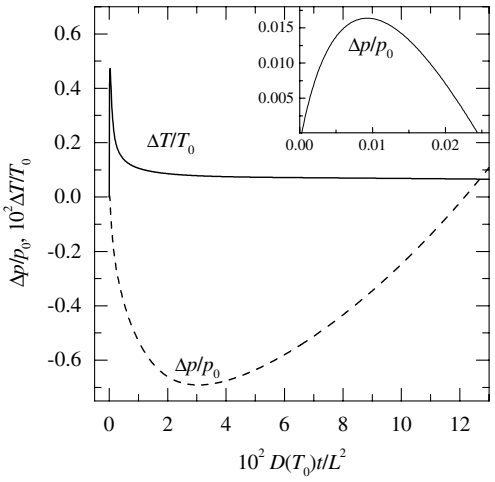


Fig. 6. An example of hydrogen absorption into a metallic tube during electrochemical hydrogen charging under potentiostatic condition. The parameters are the same as those in Fig. 2 except the convection heat loss through $H_2$ being replaced by that of $H_2O$. For comparison, the initial and applied electrode potentials induce the same $n_H$ values as those of $p_0$ and $p_1$ in Fig. 2, respectively.

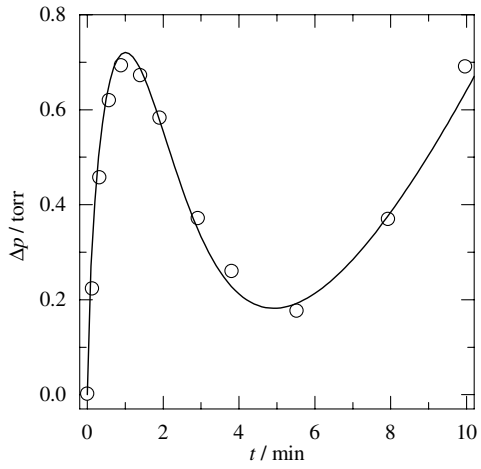


Fig. 7. Comparison of the theory with experimental results of Tong et al. [14]. The parameters: $r = 0.42$ cm, $L = 0.04$ cm, $h = 7$ cm; $V_g = 23$ cm$^3$, $p_0 = 2.1$ Torr, $p_1 = 97.0$ Torr, $T_0 = 298.15$ K; $D_0 = 4.0 \times 10^{-4}$ cm$^2$ s$^{-1}$, $E_a = 20$ kJ mol$^{-1}$, $2V_H^2 EC_0/3(1-v) = 50$ kJ mol$^{-1}$; $\Delta E_{0,+} = \Delta E_{L,+} = 25$ kJ mol$^{-1}$, $\Delta E_{0,-} = \Delta E_{L,-} = 80$ kJ mol$^{-1}$; $k_{0,+} = k_{L,+} = 1$ mol cm$^{-2}$ s$^{-1}$ Torr$^{-1}$, $b = 2 \times 10^{-6}$ Torr$^{-1/2}$; $c_M = 2.7$ J cm$^{-3}$ K$^{-1}$, $\alpha = 7.8 \times 10^{-5}$ W cm$^{-2}$ K$^{-1}$.

Eq. (19) for convenience of comparison. We find that the numerical results give good agreement with the experimental data [14]. Because our model is a more simplified one, many complicated factors are omitted; therefore this comparison is only a guide to the eye rather than based on the strict thermodynamic and kinetic parameters measured experimentally.

Of course, the present conclusion can be verified experimentally by measurement of temperature of MTW during hydrogen charging and/or discharging processes. We hope our results can stimulate the interest on this subject.

## 5. Discussion

For convenience, we deal with the heat dissipation using a simplified form of Eq. (12). The term of heat convection is only suitable for the steady state temperature profile. For the non-steady state, heat convection equations include temperatures of tube and environment, distributions of density and velocity of gas, and transports of mass and energy in the laminar area. Although the results may differ quantitatively from here, the physical picture should be the same as in this work.

For simplicity, our treatment is focused on the elastic situation and the plastic deformation being accompanied with large change of hydrogen concentration is omitted. The plastic strain will affect the distribution, concentration and transport of H in M and other properties. We will discuss it in a forthcoming paper.

We only consider the ideal solid-solution of H in M, the interaction between hydrogen atoms in metals and alloys, which causes the enthalpy $\Delta H$ changing with $n_H$ and emerging of a hydride phase, is neglected. This non-ideality will lead to amplitudes of pressure change and time interval being modified, however, the qualitative characteristics of pressure change should be the same as here.

Finally, although the present model is simple, it provides the appropriate physical picture of hydrogen transport in metals and alloys. At the same time, the present treatment could be extended to other interstitials in solid samples, e.g., lithium in Li-ion batteries, small atoms and molecules in polymers, etc. Of course, effects of enthalpy change and self-stress on other interstitial transports depend on specific situations and must be dealt with specifically.

## 6. Conclusion

Our model indicates that the pressure change during hydrogen gas diffusion into a tube is a nonequilibrium phenomenon induced by a combination of a chemical reaction, self-stress, heat and mass transports. These factors interact with each other and exhibit the super fast diffusion and up-hill diffusion before the emergence of Fickian diffusion. Appearances of super fast diffusion or up-hill diffusion depend on some parameters, e.g. the tube wall thickness, the surface activity, diffusion coefficient of hydrogen in metals and heat transport parameters; only appropriate parameter windows can exhibit all of these phenomena simultaneously. Our results also indicate that the isothermal assumption in the transport experiments is not appropriate unconditionally.

## Acknowledgment

This work is supported by NSFC Nos. 20103009, 10176030 & 10145006, and the Specialized Prophasic Basic Research Project (No. 2002CCD01900) of the Ministry of Science and Technology of China.

## References

[1] Richter D, Hempelman R, Bowman Jr RC. Dynamics of hydrogen in intermetallic hydrides. In: Schlapbach L, editor. Hydrogen in intermetallic compounds II, surface and dynamics properties, applications. Topics in applied physics, vol. 67. Berlin: Springer; 1992 [chapter 3].
[2] Wipf H, editor. Hydrogen in metals III, properties and applications. Topics in applied physics, vol. 73. Berlin: Springer; 1997. [chapters 2 and 3].
[3] Fukai Y. The metal–hydrogen system: basic bulk properties. Berlin: Springer; 1993 [chapter 5].
[4] Kirchheim R. Prog Mater Sci 1988;32:261. p. 261.
[5] Lewis FA, Magennis JP, McKee SG, Seebuwufu PJM. Nature 1983;306:673.
[6] Lewis FA, Tong XQ, Kandasamy K. Int J Hydrogen Energy 1993;18:481.

[7] Baranowski B. J Less-Common Met 1989;154:329.
[8] Sakamoto Y, Tong XQ, Lewis FA. Scripta Metall Mater 1991;25:1629.
[9] Kandasamy K, Lewis FA, Magennis JP, McKee SG, Tong XQ. Z Phys Chem NF 1991;171:213.
[10] Tong XQ, Kandasamy K, Lewis FA. Scripta Metall 1990;24:1923.
[11] Tong XQ, Bucur RV, Kandasamy K, Lewis FA. Z Phys Chem NF 1993;181:225.
[12] Tong XQ, Lewis FA. Int J Hydrogen Energy 1995;20:641.
[13] Lewis FA, Baranowski B, Kandasamy K. J Less-Common Met 1987;134:L27.
[14] Tong XQ, Lewis FA. J Less-Common Met 1991;169:157.
[15] Tong XQ, McNicholl R-A, Kandasamy K, Lewis FA. Int J Hydrogen Energy 1992;17:777.
[16] Kandasamy K, Tong XQ, Lewis FA. J Phys Conden Mater 1992;4:L439.
[17] Dudek D, Baranowski B. Polish J Chem 1995;69:1196.
[18] De Ninno A, Violante V, La Barbera A. Phys Rev B 1997;56:2417.
[19] Legawiec B, Zoltowski P. J Phys Chem B 2002;106:4933.
[20] Zhang WS, Zhang XW, Zhang ZL. Phys Rev B 2000;62:8884.
[21] Zhang WS, Zhang XW, Zhang ZL. J Alloys Compd 2000; 302:258.
[22] Zhang WS, Zhang ZL, Zhang XW. J Alloys Compd 2002;336:170.
[23] Zhang WS, Zhang ZL, Zhang XW. J Alloys Compd 2002;346:176.
[24] Zhang WS. J Alloys Compd 2003;356–357:314.
[25] Adrover A, Giona M, Capobianco L, Tripodi P, Violante V. Int J Hydrogen Energy 2003;28:1279.
[26] Hickman RG. J Less-Common Met 1969;19:369.
[27] Baranowski B. Diffusion in elastic media with stress fields. In: Sieniutycz S, Salaman P, editors. Advances in thermodynamics flow diffusion and processes, vol. 6. New York: Taylor Francis; 1992. p. 168.
[28] Baranowski B, Majchrzak S, Flanagan TB. J Phys F Met Phys 1971;1:258.
[29] Kirchheim R. Acta Metall 1986;34:37.
[30] Timoshenko S. Strength of materials: part II advanced theory and problems. 3rd ed. Princeton, NJ: D. Van Nostrand Company Inc; 1956. p. 125.
[31] Eckert ERG, Drake RM. Analysis of heat and mass transfer. Columbus, OH: McGraw-Hill; 1972 [chapter 15].
[32] Kutateladze SS. Analysis of similarity in thermo-physics. Novosibirsk USSR: Science Publishers Siberian Division; 1982 [chapter 4 (in Russian)].
[33] Assael MJ, Mixafendi S, Wakeham WA. J Phys Chem Ref Data 1986;15:1315. p. 1315.
[34] Zhang WS, Zhang ZL, Zhang XW. J Electroanal Chem 1999;474:130.